

Shear Thickening Oscillation in a Dilatant Fluid

Hiizu NAKANISHI and Namiko MITARAI¹

Department of Physics, Kyushu University 33, Fukuoka 812-8581, Japan

¹*Niels Bohr Institute, University of Copenhagen, Blegdamsvej 17, DK-2100 Copenhagen Ø, Denmark*

(Received November 17, 2010; accepted January 11, 2011; published online February 25, 2011)

By introducing a state variable, we construct a phenomenological fluid dynamical model of a dilatant fluid, i.e., a dense mixture of fluid and granules that shows severe shear thickening. We demonstrate that the fluid shows shear thickening oscillation, namely, the fluid flow oscillates owing to the coupling between the fluid dynamics and the internal dynamics of state. We also demonstrate that the jamming leads to a peculiar response to an external impact on the fluid.

KEYWORDS: dilatant fluid, fluid dynamics, shear thickening, jamming, oscillatory instability

A dense mixture of starch and water is an ideal material for demonstrating the shear thickening property of a non-Newtonian fluid. It may behave as liquid but immediately solidifies upon sudden application of stress; thus, one can even run over a pool filled with this fluid. It is intriguing to see that it develops protrusions on its surface when subjected to strong vertical vibrations,^{1,2)} and that it vibrates spontaneously when poured it out of a container. One source of these unusual behaviors is severe shear thickening; the viscosity of the fluid increases almost discontinuously by almost three orders of magnitude at a certain critical shear rate,³⁾ which makes the fluid behave like a solid upon abrupt deformation. Such severe shear thickening is often found in dense colloid suspensions and granule–fluid mixtures,⁴⁻⁷⁾ which have sometimes been called “dilatant fluids” owing to their apparent analogy to granular media showing Reynolds dilatancy.⁸⁾

Despite its suggestive name, physicists have not reached a microscopic understanding for the shear thickening property of the dilatant fluid. It was originally proposed that the shear thickening is owing to the order–disorder transition of dispersed particles;^{4,5,9,10)} the viscosity increases when the fluid flow in high-shear regimes destroys the layered structure in lower-shear regimes. Although there seem to be some situations where this mechanism is responsible for the shear thickening, there are other cases where the layered structure is not observed prior to the shear thickening¹¹⁾ or where no significant changes in the particle ordering are found upon the discontinuous thickening.^{12,13)} Cluster formation owing to hydrodynamic interaction¹⁴⁻¹⁷⁾ and jamming^{3,6,18-22)} have been proposed as plausible mechanisms.

There are several remarkable features of the shear thickening shown by a dilatant fluid: (i) the thickening is so severe and instantaneous that it might be used even to make a body armor to stop a bullet,²³⁾ (ii) the relaxation after the removal of the external stress occurs within a few seconds, which is not slow but neither as instantaneous as that in the thickening process, (iii) the thickened state is almost rigid and does not allow much elastic deformation unlike the state of a viscoelastic material, (iv) the viscosity shows hysteresis upon changing the shear rate,⁷⁾ and (v) noisy fluctuations have been observed in response to an external shear stress in the thickening regime.^{7,22)}

In this study, we construct a phenomenological model at the macroscopic level and examine the fluid dynamical

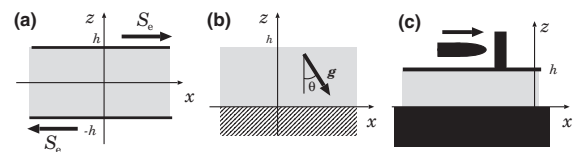


Fig. 1. Flow configurations with the coordinate system: (a) simple shear flow, (b) gravitational slope flow, and (c) impact-driven flow, where the upper wall is mobilized by a bullet impact.

behavior of a dilatant fluid. We introduce a state variable that describes an internal state of the fluid phenomenologically, and couple its dynamics with fluid dynamics. We find that the following two aspects of the model are important: (1) the fluid state changes in response to the shear stress, (2) the state variable changes proportionally to the shear rate. We examine the model behavior in simple configurations, and demonstrate that the model is capable of describing the characteristic features of hydrodynamic behavior and that the fluid shows *shear thickening oscillation*.

Model: Our model is based on the incompressible Navier–Stokes equation with the viscosity $\eta(\phi)$ that depends on the state variable ϕ . The scalar field ϕ , which takes a value of $[0, 1]$, represents the local state of the medium. We assume two limiting states: the low-viscosity state ($\phi \sim 0$) and high-viscosity state ($\phi \sim 1$). At $\phi = 1$, the system is supposed to be jammed and the viscosity diverges.

The state variable ϕ relaxes to a steady value ϕ_* determined by the local shear stress S ; ϕ_* is supposed to be continuous and monotonically increasing from 0 to ϕ_M as a function of S with a characteristic stress S_0 . The limiting value ϕ_M represents the state of the medium in the high stress limit and should depend on the medium properties such as the packing fraction of dispersed granules. In the following, we employ the forms

$$\eta(\phi) = \eta_0 \exp\left[\frac{A\phi}{1-\phi}\right], \quad \phi_*(S) = \phi_M \frac{(S/S_0)^2}{1 + (S/S_0)^2} \quad (1)$$

with a dimensionless constant A . The Vogel–Fulcher type divergence is assumed in $\eta(\phi)$ in order to represent the severe thickening.

For the simple shear flow configuration shown in Fig. 1(a) with the flow field given by

$$\mathbf{v} = (u(z, t), 0, 0), \quad (2)$$

the dynamics is described by the following set of equations:

$$\rho \frac{\partial u(z, t)}{\partial t} = \frac{\partial}{\partial z} S(z, t), \quad (3)$$

$$\frac{\partial \phi(z, t)}{\partial t} = -\frac{1}{\tau} (\phi(z, t) - \phi_*(S(z, t))), \quad (4)$$

with ρ and τ being the medium density and relaxation time, respectively. The shear stress $S(z, t)$ is given by

$$S(z, t) = \eta(\phi) \dot{\gamma}, \quad \dot{\gamma} \equiv \frac{\partial u}{\partial z}, \quad (5)$$

where the shear rate is denoted by $\dot{\gamma}$.

Now, we suppose that the relaxation of ϕ toward ϕ_* is driven by the shear deformation; thus, the relaxation rate $1/\tau$ is not constant but proportional to the absolute value of the shear rate, i.e.,

$$\frac{1}{\tau} = \frac{|\dot{\gamma}|}{r} \quad (6)$$

with a dimensionless parameter r . Note that, with this form of relaxation, the state variable ϕ does not exceed 1 even when $\phi_M > 1$ because $\dot{\gamma} \rightarrow 0$ as $\phi \nearrow 1$ owing to the diverging viscosity.

This form of relaxation is natural for the athermal relaxation driven by local deformation. The system responds in accordance with the deformation rate, and does not change the state unless it deforms. This should be valid if the state change is caused by local configurational changes of the dispersed granules owing to medium deformation, unless Brownian motion plays an important role.

In the following, numerical results are given in the dimensionless unit system, where $\eta_0 = S_0 = \rho = 1$, i.e., the time, length, and mass units are respectively given as

$$\tau_0 = \frac{\eta_0}{S_0}, \quad \ell_0 = \sqrt{\frac{\eta_0 \tau_0}{\rho}}, \quad m_0 = \rho \ell_0^3. \quad (7)$$

For the cornstarch suspension of 41 wt%,³⁾ these may be estimated as $S_0 \approx 50$ Pa, $\eta_0 \approx 10$ Pa·s, and $\rho \approx 10^3$ kg/m³, which give $\tau_0 \approx 0.2$ s and $\ell_0 \approx 5$ cm.

Steady shear flow: First, we examine the model behavior in the steady shear flow configuration with a fixed external stress S_e [Fig. 1(a)]. The boundary condition is then given by

$$S_e = S(z, t)|_{z=\pm h}. \quad (8)$$

The steady state solution for eqs. (3) and (4) with this boundary condition is obtained easily as

$$\phi = \phi_*(S_e), \quad \dot{\gamma} = \frac{S_e}{\eta(\phi_*)} \equiv \dot{\gamma}_*(S_e). \quad (9)$$

The stress–shear rate curves are plotted in Fig. 2 for ϕ_* and $\eta(\phi)$ of eq. (1) with $A = 1$ for various values of ϕ_M . In the logarithmic scale, the straight line with the slope 1 corresponds to the linear relation with a constant viscosity. In the curve for $\phi_M = 0.8$, one can see two regimes: the low-viscosity regime and high-viscosity regime. Between the two regimes, there is an unstable region. From the stress–shear rate curve, we expect to observe hysteresis upon changing the shear rate $\dot{\gamma}$ with discontinuous jumps between the two branches. The jumps correspond to the discontinuous change in viscosity, i.e., the abrupt shear thickening. In the case of $\phi_M \geq 1$, the curves do not have an upper linear branch because the viscosity diverges and the fluid solidifies.

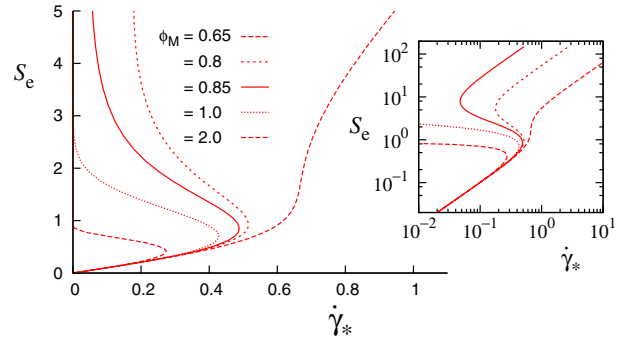


Fig. 2. (Color online) Stress–shear rate relation for the viscosity given by eq. (1) with $A = 1$. The inset shows the same plots in the logarithmic scale.

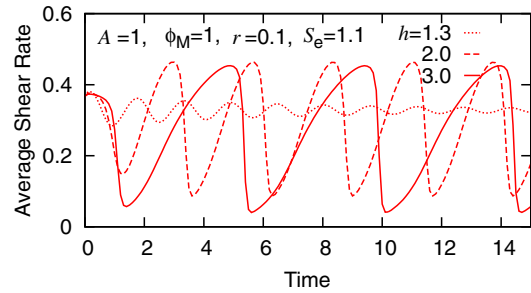


Fig. 3. (Color online) Oscillations of the average shear rate $u(h)/h$ in shear flow for $h = 1.3, 2,$ and 3 with $A = \phi_M = 1, r = 0.1,$ and $S_e = 1.1$. The initial state is chosen as the steady state solution (9) with $S_e = 1.0$ at $t = 0$.

Shear thickening oscillation: If the external stress S_e is kept at a value in the unstable branch, where

$$\frac{d\dot{\gamma}_*}{dS_e} < 0, \quad (10)$$

i.e., the shear rate decreases as the stress increases, the steady flow may become unstable. The linear stability analysis with the perturbation $\delta v = (\delta u, 0, 0)e^{i(kz - \omega t)}$ shows that the mode whose wave number k in the z -axis satisfies

$$0 < k^2 < \rho \frac{\dot{\gamma}_*}{r} \left[-\frac{d\dot{\gamma}_*}{dS_e} \right] \equiv k_c^2 \quad (11)$$

grows and that the threshold mode k_c oscillates at the finite frequency

$$\omega_c = \sqrt{\frac{S_e}{\rho r}} k_c. \quad (12)$$

Since the smallest possible wave number k_{\min} is given by $k_{\min} = \pi/(2h)$, we expect the oscillatory flow to appear for $k_{\min} < k_c$ as the system width increases if the external stress is in the unstable branch.

The oscillatory behavior of the shear flow in the unstable regime can be seen by numerically integrating eqs. (3) and (4) with eq. (8). In Fig. 3, the average shear rate $u(h)/h$ is plotted as a function of time for some values of the system width $2h$ for $\phi_M = A = 1$ and $r = 0.1$ with the external shear stress $S_e = 1.1$ in the unstable regime. The initial state is chosen as the steady solution (9) with $S_e = 1$. In the case of $h = 1.3$, one can see the overdamped oscillation that converges to the steady state, but for larger values of h , the

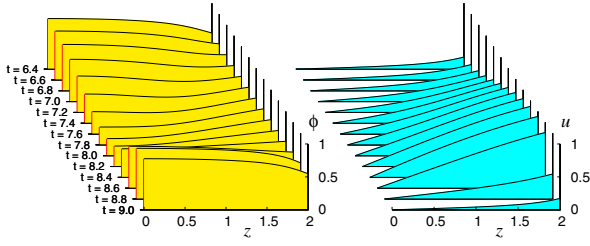


Fig. 4. (Color online) Spatial variation of shear flow oscillation for $A = \phi_M = 1$, $r = 0.1$, $S_c = 1.1$, and $h = 2$.

system undergoes the oscillatory transition, and the surface velocity oscillates with a sawtooth-like wave profile, namely, a gradual increase in velocity followed by a sudden drop.

The time developments of the spatial variations for the state variable ϕ and the velocity u are plotted in Fig. 4. Only the positive halves ($z > 0$) of the symmetric solutions are shown. One can see that the high-shear-rate region extends gradually towards the center as ϕ relaxes, then the velocity drops suddenly to a very small value when the shear rate exceeds a certain value and ϕ increases rapidly. This sudden drop in velocity is owing to the abrupt thickening of the fluid caused by the high shear stress. The resulting low shear rate eventually leads to the low shear stress, which in turn leads to small ϕ with a low viscosity; then the shear rate increases again.

Gravitational flow: The gravitational flow in Fig. 1(b) is examined using eq. (2) by adding the body force term to eq. (3) due to gravity,

$$\mathbf{g} = (g \sin \theta, 0, -g \cos \theta) \equiv (g_{\parallel}, 0, g_{\perp}), \quad (13)$$

with the boundary condition

$$u(0, t) = 0, \quad S(h, t) = 0. \quad (14)$$

The steady flow profiles $u(z)$ are shown in Fig. 5(a) for various g_{\parallel} values with a depth $h = 2$. For a small g_{\parallel} , the profile is nearly parabolic as in a Newtonian fluid, but for a larger g_{\parallel} , an inflection point appears in $u(z)$. One notable feature is that the flow velocity is lower for a larger g_{\parallel} . This can also be seen in Fig. 5(b), where the surface velocity $u(h)$ is plotted against g_{\parallel} . This is a direct consequence of the shear stress thickening.

The part where $u''(z) > 0$ corresponds to the unstable branch in the stress–shear rate curve. Thus, we may expect the shear thickening oscillation, as in the simple shear flow. In Fig. 5(c), the surface velocity is plotted as a function of time. One can see the oscillation as soon as the inflection point appears, but for a large g_{\parallel} , the oscillation overdamps owing to the large viscosity.²⁴⁾

Response to impact: The athermal relaxation (6) gives the system an interesting feature in response to an external impact. We consider the simple shear flow with the fixed lower boundary at $z = 0$, but the upper boundary at $z = h$ is forced to move at a velocity u_0 at $t = 0$ [Fig. 1(c)]. For $t > 0$, the velocity of the upper wall $U(t) \equiv u(h, t)$ is given by

$$m \frac{dU(t)}{dt} = -\eta(\phi) \left. \frac{\partial u}{\partial z} \right|_{z=h}, \quad (15)$$

where m is the mass of the upper wall per unit length.

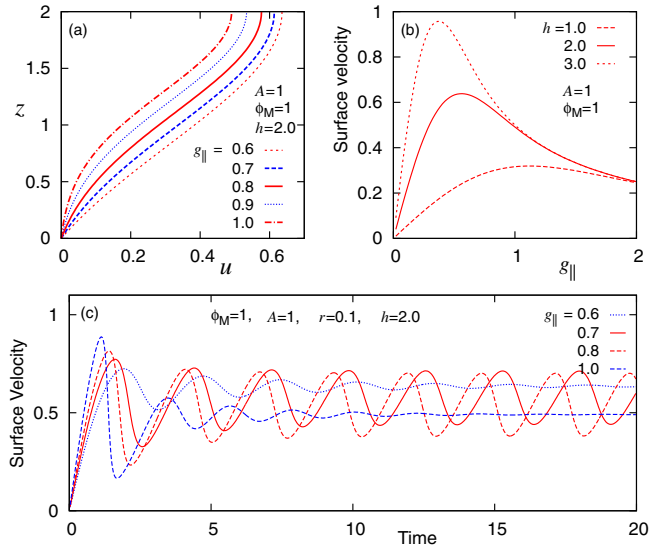


Fig. 5. (Color online) Gravitational flows: (a) Flow profile of steady flow for various g_{\parallel} values with $h = 2$. (b) Surface velocity as a function of g_{\parallel} for $h = 1, 2$, and 3 . (c) Time dependences of surface velocity for $g_{\parallel} = 0.6, 0.7, 0.8$, and 1.0 with $h = 2$. The other parameters are $A = \phi_M = 1$ and $r = 0.1$.

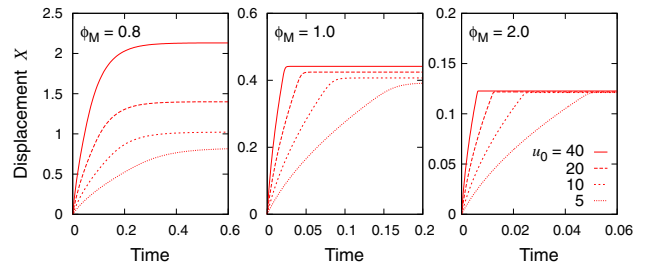


Fig. 6. (Color online) Time dependences of the displacement X after the impact with the initial speeds $u_0 = 40, 20, 10$, and 5 for the system with $\phi_M = 0.8, 1$, and 2 . The other parameters are $h = 2$, $A = 1$, $r = 0.1$, and $m = 1$.

Figure 6 shows the displacement X of the upper wall,

$$X(t) = \int_0^t U(t') dt', \quad (16)$$

in the three cases of $\phi_M = 0.8, 1$, and 2 for various initial speeds. The wall decelerates rapidly as the fluid thickens owing to the imposed stress, and eventually stops. For $\phi_M = 0.8$, the final wall distance increases as the initial speed u_0 increases. On the other hand, for $\phi_M = 2$, the final displacement does not depend on u_0 . This is because the fluid gets jammed at a certain strain as it deforms, and cannot deform further.

Concluding remarks: We have constructed a phenomenological model of the dilatant fluid, and demonstrated that the fluid may show the shear thickening oscillation. The athermal relaxation gives the fluid the feature that its deformation does not depend on the strength of the applied impact.

A couple of models have been proposed for the shear thickening fluid: the soft glassy rheology (SGR) model²⁵⁾ and the schematic mode coupling theory (MCT).²⁶⁾ In the SGR model, SGR is extended to describe the shear thickening by introducing the stress-dependent effective

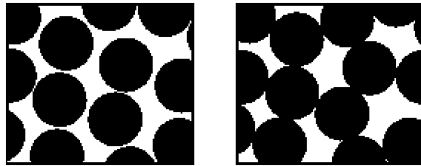


Fig. 7. Schematic illustrations of configurations for low-stress (left) and high-stress (right) regimes.

temperature, which may be compared with the inverse of the state variable ϕ of our model. In the schematic MCT, the jamming transition has been examined using MCT, incorporating the effects of shear schematically. Both are semiempirical but deal with microscopic processes and produce the similar flow curves similar to those in Fig. 2. In contrast, the present model is phenomenological only for macroscopic description, and we study the interplay between the fluid dynamics and the shear thickening.

Although our model is phenomenological, we have a microscopic picture of the system. In the low-stress regime ($\phi \sim 0$), the particles are dispersed, thus, the medium can deform easily owing to the lubrication. However, in the high-stress regime ($\phi \sim 1$), the particles form contacts and force chains to support the stress, and eventually the fluid get jammed when the packing fraction is large enough (Fig. 7). With this picture, it is natural to assume that the time scale for the state change is set by the shear rate in the case where the deformation drives the configurational changes, and then the parameters S_0 and r correspond to the stress and the strain, respectively, around which the neighboring granules start to come into contact with each other. In the case where the thermal relaxation also takes place, the time scale may be given by

$$\frac{1}{\tau} = \frac{|\dot{\gamma}|}{r} + \frac{1}{\tau_{\text{th}}}, \quad (17)$$

where τ_{th} is the time scale at which the thermal agitation severs the contact.

We have assumed that the state is determined by the shear stress, but it is instructive to consider the case where the state is determined by the shear rate. If ϕ_* is a function of $\dot{\gamma}$ instead of eq. (1), the stress–shear rate curve becomes monotonically increasing without an unstable branch. As a result, there should be no discontinuity or hysteresis, and thus no instability that leads to the oscillation. This suggests that the experimentally observed discontinuous transition³⁾ and hysteresis⁷⁾ can be attributed to the “shear–stress thickening” property of the medium. The direct consequence of the shear–stress thickening is seen in the gravitational slope flow, where the flux does not increase monotonically with the inclination angle because the fluid becomes more viscous under a larger shear stress; thus, it may flow slower as the slope becomes steeper.

A remarkable result of the present model is the oscillatory instability in the shear and the gravitational flow. Superficially, this may look like a stick-slip motion, but its physical origin is different; the stick-slip motion is caused by the slip weakening friction in a system driven at a constant speed by an elastic device. If the present system is driven at a constant speed, the system settles in one of the stable states for a given $\dot{\gamma}$. The oscillatory behavior in the present system appears under the

drive with a constant shear stress, and it is a result of the coupling between the internal dynamics and the fluid dynamics. In this sense, it is also different from the oscillation in the SGR model, where the fluid dynamics is not considered.²⁵⁾

Regarding the oscillations in the experiments, one can easily notice the vibration at approximately 10 Hz when pouring the cornstarch–water mixture out of a cup. In the literature, the pronounced fluctuations in the deformation rate have been reported in the shear–stress-controlled experiment near the critical shear rate,^{7,22)} but not many experiments have been reported yet. On the other hand, in the case of the shear thinning system, a much clearer oscillation has been reported in the liquid crystal systems²⁷⁾ along with discontinuous transition and hysteresis,^{28,29)} which may be described by a phenomenology similar to the present one.

Chaotic dynamics has been observed in dilute aqueous solutions of a surfactant in an experiment under a constant shear rate in the shear thickening regime.^{30,31)} It was interpreted as the stick-slip transition between the two states of the fluid structure; thus, its physical relevance to the present instability is not clear. However, we also found the chaotic dynamics in the present model in the case of a constant relaxation time τ with a large system width.

Acknowledgement This work was supported by a Grant-in-Aid for Scientific Research (21540418).

- 1) F. S. Merkt, R. D. Deegan, D. I. Goldman, E. C. Rericha, and H. L. Swinney: *Phys. Rev. Lett.* **92** (2004) 184501.
- 2) H. Ebata, S. Tatsumi, and M. Sano: *Phys. Rev. E* **79** (2009) 066308.
- 3) A. Fall, N. Huang, F. Bertrand, G. Ovarlez, and D. Bonn: *Phys. Rev. Lett.* **100** (2008) 018301.
- 4) R. Hoffman: *Trans. Soc. Rheol.* **16** (1972) 155.
- 5) H. Barnes: *J. Rheol.* **33** (1989) 329.
- 6) E. Brown and H. M. Jaeger: *Phys. Rev. Lett.* **103** (2009) 086001.
- 7) H. Laun, R. Bung, and F. Schmidt: *J. Rheol.* **35** (1991) 999.
- 8) O. Reynolds: *Philos. Mag.* **S5** (1885) 469.
- 9) R. Hoffman: *J. Colloid Interface Sci.* **46** (1974) 491.
- 10) R. Hoffman: *J. Rheol.* **42** (1998) 111.
- 11) H. Laun, R. Bung, K. Hahn, E. Hädicke, R. Hingmann, F. Schmidt, S. Hess, W. Loose, O. Hess, and P. Lindner: *J. Rheol.* **36** (1992) 743.
- 12) B. J. Maranzano and N. J. Wagner: *J. Chem. Phys.* **117** (2002) 10291.
- 13) R. G. Egres and N. J. Wagner: *J. Rheol.* **49** (2005) 719.
- 14) J. Brady and G. Bossis: *J. Fluid Mech.* **155** (1985) 105.
- 15) J. Bender and N. J. Wagner: *J. Rheol.* **40** (1996) 899.
- 16) B. J. Maranzano and N. J. Wagner: *J. Chem. Phys.* **114** (2001) 10514.
- 17) J. Melrose and R. Ball: *J. Rheol.* **48** (2004) 937.
- 18) J. Melrose and R. Ball: *J. Rheol.* **48** (2004) 961.
- 19) R. Farr, J. Melrose, and R. Ball: *Phys. Rev. E* **55** (1997) 7203.
- 20) M. E. Cates, J. P. Wittmer, J.-P. Bouchaud, and P. Claudin: *Phys. Rev. Lett.* **81** (1998) 1841.
- 21) E. Bertrand, J. Bibette, and V. Schmitt: *Phys. Rev. E* **66** (2002) 060401.
- 22) D. Lootens, H. van Damme, Y. Hémar, and P. Hébraud: *Phys. Rev. Lett.* **95** (2005) 268302.
- 23) N. J. Wagner and J. F. Brady: *Phys. Today* **62** [10] (2009) 27.
- 24) This inflection point criterion has nothing to do with Rayleigh’s inflection point theorem.
- 25) D. A. Head, A. Ajdari, and M. E. Cates: *Phys. Rev. E* **64** (2001) 061509.
- 26) C. B. Holmes, M. E. Cates, M. Fuchs, and P. Sollich: *J. Rheol.* **49** (2005) 237.
- 27) A. S. Wunenburger, A. Colin, J. Leng, A. Arnéodo, and D. Roux: *Phys. Rev. Lett.* **86** (2001) 1374.
- 28) D. Bonn, J. Meunier, O. Greffier, A. Al-Kahwaji, and H. Kellay: *Phys. Rev. E* **58** (1998) 2115.
- 29) O. Volkova, S. Cutillas, and G. Bossis: *Phys. Rev. Lett.* **82** (1999) 233.
- 30) R. Bandyopadhyay, G. Basappa, and A. K. Sood: *Phys. Rev. Lett.* **84** (2000) 2022.
- 31) R. Bandyopadhyay and A. K. Sood: *Europhys. Lett.* **56** (2001) 447.